LIMNOLOGY
and
OCEANOGRAPHY

ASLO

*Limnol. Oceanogr.* 00, 2017, 00–00
© 2017 The Authors Limnology and Oceanography published by Wiley Periodicals, Inc.
on behalf of Association for the Sciences of Limnology and Oceanography
doi: 10.1002/lno.10648

# Seasonal changes in the biochemical fate of carbon fixed by benthic diatoms in intertidal sediments

**Tanja C. W. Moerdijk-Poortvliet,[1,2]* Peter van Breugel,[1] Koen Sabbe,[3] Olivier Beauchard,[4,5] Lucas J. Stal ,[1,6] Henricus T. S. Boschker[1]**

[1]Department of Marine Microbiology and Biogeochemistry and Utrecht University, NIOZ Royal Institute for Sea Research, Den Burg, The Netherlands
[2]Chemistry Department, HZ University of Applied Sciences, Vlissingen, The Netherlands
[3]Biology Department, Laboratory of Protistology and Aquatic Ecology, Ghent University, Ghent, Belgium
[4]Flanders Marine Institute (VLIZ), InnovOcean site, Oostende, Belgium
[5]Department of Biology, University of Antwerp, Antwerpen, Belgium
[6]Department of Aquatic Microbiology, University of Amsterdam, Amsterdam, The Netherlands

## *Abstract*

Benthic diatoms are important primary producers in intertidal marine sediments and form the basis of the food web in these ecosystems. In order to investigate the carbon flow within diatom mats, we performed in situ $^{13}C$ pulse-chase labeling experiments and followed in detail the biochemical fate of carbon fixed by the diatoms for five consecutive days. These labeling experiments were done at approximately 2-monthly intervals during 1 yr in order to cover seasonal variations. The fixed carbon was recovered in individual carbohydrates including extracellular polymeric substances (EPS), amino acids, fatty acids, and nucleic acid bases. In addition, we assessed a variety of environmental parameters and photosynthetic characteristics. The fixed carbon was initially mainly stored as carbohydrate (glucose) while nitrogen-rich compounds (e.g., amino acids and RNA/DNA) were produced more slowly. During the year, the diatoms distributed the photosynthetically fixed carbon differently among the various carbon pools that were measured. In summer, the diatoms decreased carbon fixation and accumulated relatively more lipid as a storage compound (27% ± 2% vs. 12% ± 5% in other seasons). The percentage of fixed carbon that was excreted as EPS was lower in summer compared to other seasons, amounting 9% ± 4% and 21% ± 6%, respectively. Hence, it seemed that the physiology of the microphytobenthos was different during summer and caused by higher light intensity and a shift in nitrogen source.

Microphytobenthos on intertidal mudflats may contribute up to 50% of the total primary production within estuaries (Cahoon 1999; Underwood and Kromkamp 1999). In temperate regions, diatoms are the dominant group in microphytobenthic communities and can form dense mats at the sediment surface (Admiraal et al. 1984; MacIntyre and Cullen 1996). These mats provide a major source of carbon for the successive trophic levels, including microbes (Herman et al. 2000; Middelburg et al. 2000; Taylor et al. 2013; Como et al. 2014).

Benthic diatoms achieve high rates of photosynthesis (Pniewski et al. 2015). Depending on the nutrient status of the diatom mats the initially produced glucose can be used for the biosynthesis of cellular compounds such as other carbohydrates (CHO), amino acids (AA), fatty acids (FA) and nucleic acids. For example, under nutrient replete conditions up to 40% of the photosynthetically fixed carbon may be directed toward the synthesis of AAs (Levitan et al. 2015). However, as available nutrients may be limiting in compact diatom mats, fixed carbon may be initially stored as the reserve polymer chrysolaminaran (1,3-D-glucan) that may be converted into other cellular components once nutrients become available (Kroth et al. 2008; Bellinger et al. 2009). Moreover, under nitrogen deficiency (or under the photo-oxidative stress that is the consequence of nitrogen depletion) or other adverse environmental conditions, the intermediate metabolism is altered and the fate of fixed carbon is directed to triglycerides, which may also serve as a storage compound (Hu et al. 2008; Hockin et al. 2012). However, space for intracellular storage of reserve compounds is obviously limited and therefore excess fixed carbon can also be

*Correspondence: tanja.moerdijk@gmail.com

Additional Supporting Information may be found in the online version of this article.

This is an open access article under the terms of the Creative Commons Attribution License, which permits use, distribution and reproduction in any medium, provided the original work is properly cited.

exuded as EPS, which may explain up to 73% of the carbon fixation (Goto et al. 1999; Smith and Underwood 2000; Underwood and Paterson 2003).

Diatoms are able to utilize a variety of inorganic nitrogen sources (e.g., nitrate, ammonium) and organic nitrogen sources (e.g., urea, AAs) and adjust their nitrogen metabolism according to the available nutrients, which may either be supplied from the sediment or from the water during high tide (Bender et al. 2012). The presence of a metazoan-like urea cycle in the genome of diatoms came as a surprise (Armbrust et al. 2004). Although the functioning of the urea cycle in diatoms is not completely understood it is assumed to be involved in the recycling and biosynthesis of organic nitrogen compounds and important for the exchange of nutrients between the mitochondria and the cytoplasm (Allen et al. 2011; Prihoda et al. 2012). The urea cycle may therefore play a role in the metabolic response of diatoms to changes in nutrient availability. The fate of carbon fixed by benthic diatoms will also change as the result of seasonal variation in environmental conditions (e.g., nutrient availability, temperature, and light intensity) and this could affect the overall functioning of the diatom mat. Moreover, when diatoms experience stress due to low nutrient availability or high light intensities and react by storing carbon in the form of chrysolaminaran and/or triglycerides (i.e., compounds rich in carbon, but lacking nitrogen or phosphorus) the nutritional value of the diatoms will decline for higher trophic levels. Eventually, food web structure might be affected, which will have its effect on the functioning of the whole ecosystem (van Oevelen et al. 2006).

Stable isotope labeling techniques are a valuable tool to study the carbon cycle in intertidal mudflats. With these techniques, organic carbon cycling and the classical food web have been well studied (Herman et al. 1999; Degré et al. 2006; van Oevelen et al. 2006). However, only a few studies focused on carbon flows within diatom mats. The majority of studies dealt with various aspects of lipid biochemistry because of the inability of established techniques to study other metabolites (Middelburg et al. 2000; Bouillon and Boschker 2006; Evrard et al. 2008; Bellinger et al. 2009). The development of a new compound-specific stable isotope technique enabled the unraveling of metabolic pathways of photosynthetically acquired carbon in benthic diatoms (Moerdijk-Poortvliet et al. 2014*a*). Liquid Chromatography Isotope Ratio Mass Spectrometry (LC/IRMS) was applied to study CHO metabolism in diatom mats by Oakes et al. (2010) and by Miyatake et al. (2014). The development of additional LC/IRMS methods for AAs and nucleic acids allows the study of all major classes of biological compounds, which improved our insight in the functioning of diatom mats (Boschker et al. 2008; Moerdijk-Poortvliet et al. 2014*a*,*b*).

Because environmental conditions such as temperature, light intensity, and nutrient availability vary between seasons, we hypothesized that during the course of a year the physiology of benthic diatoms is different and as a result the partitioning of fixed carbon between the major metabolic pools (i.e., CHOs, FAs, AAs, and nucleic acids) changes. To test this hypothesis, six in situ $^{13}C$ pulse-chase experiments were carried out in order to trace the carbon flow in an intertidal diatom mat for 5 d at intervals of approximately 2 months during 1 yr. We also monitored a variety of environmental parameters, such as light, temperature and nutrient concentrations, and measured photosynthetic parameters. This approach provided information on the rate of biosynthesis of the different carbon compounds and the subsequent turnover due to transfer between the different carbon pools as well as losses from the system in relation to environmental conditions. Nevertheless, several important carbon pools stayed outside our analytical window. These included amino sugars, lectins, acidic CHOs, pigments, and quinones, which may have contributed to an incomplete recovery of the $^{13}C$-label.

## Methods

### Study site and in situ $^{13}C$ labeling experiments

In 2011, six in situ $^{13}C$-labeling experiments were carried out every 2 months at the Zandkreek intertidal mudflat, which is situated along the southern shore of the Oosterschelde estuary in the Southwest of the Netherlands (51°32′41″N, 3°53′22″E). The sampling site was located 0.15 m below the mean tidal level and the emersion period was approximately 6 h per tidal cycle. The silt content of the sediment (fraction $< 0.63$ $\mu$m particle size) was $26\% \pm 3\%$ and the median grain size was $103 \pm 8$ $\mu$m, which did not change during the year. Also, the water content of the sediment did not change during the year and varied between 29% and 34%. Seasonal changes in the average temperature in the top 15 mm of the sediment during labeling and the photosynthetic active radiation (PAR) are shown in Fig. 1. During winter the intertidal mudflat developed transient diatom mats, which disappeared during summer although the presence of diatoms at the sediment surface was visible throughout the year.

Sediment organic carbon content showed small differences during the year and varied between $4844 \pm 120$ mmol $m^{-2}$ and $6588 \pm 37$ mmol $m^{-2}$. Bioturbating fauna such as the amphipod crustacean *Corophium volutator* and the hydrobiid snail *Peringia ulvae* developed in late spring (June) presumably resulting in higher grazing rates and a more mixed sediment top layer during summer (Herman et al. 2000).

Experiments were started immediately after emersion of the mudflat. Two $0.5 \times 0.5$ $m^2$ stainless steel frames were pushed into the sediment to a depth of 80 mm in order to constrain the labeling and sampling area. The two frames were treated as duplicates ($n = 2$) and were divided in a $100 \times 100$ $mm^2$ sampling grid. Unlabeled control samples

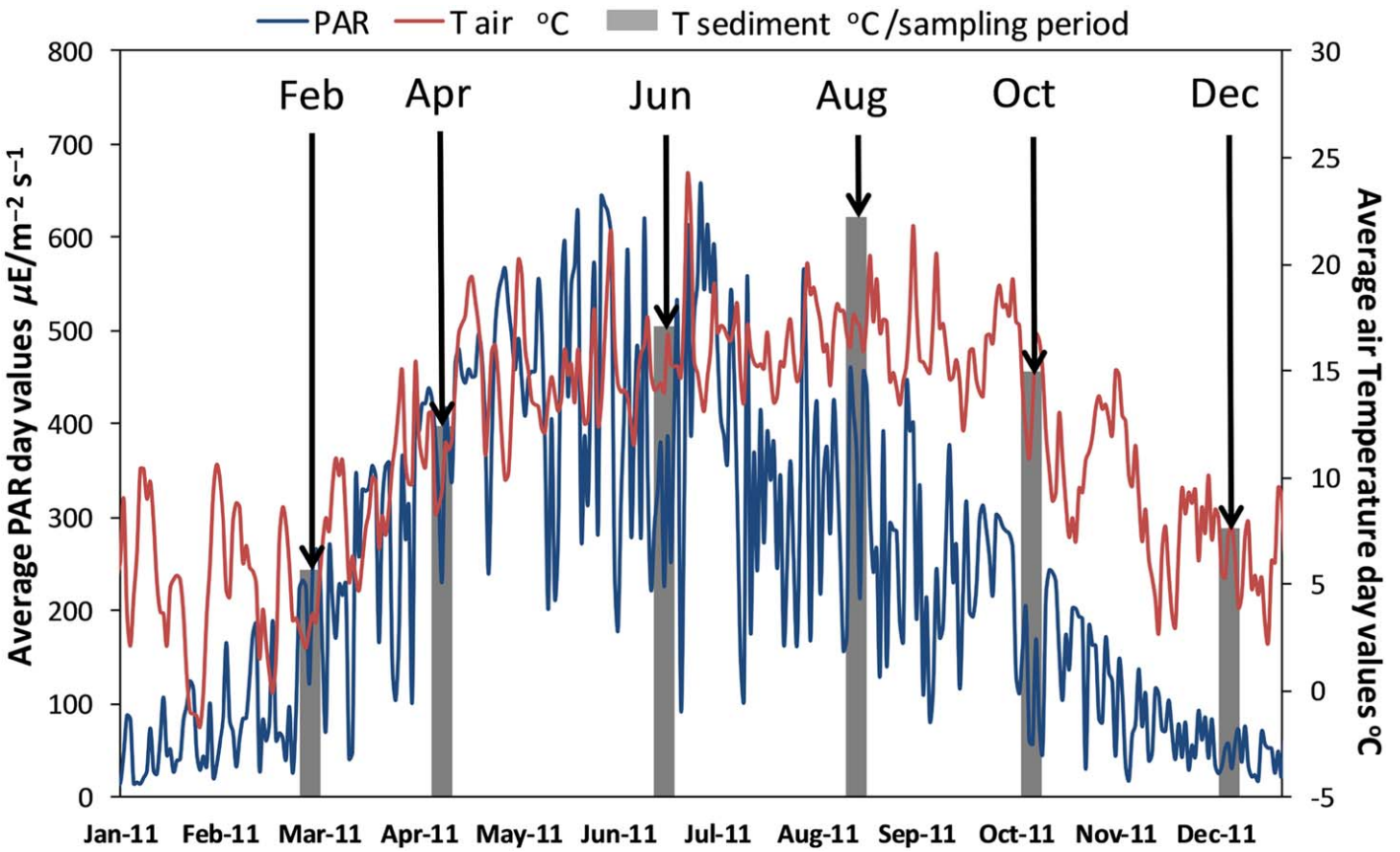


**Fig. 1.** Annual photosynthetically active radiation (PAR) and air temperature. The position of the bars indicates the sampling period and the height indicates the average sediment temperature during the pulse-labeling period.

were taken just outside the frames as described below. The in situ labeling experiment was started by spraying the surface of the sediment within each frame with 200 mL of [$^{13}$C] sodium bicarbonate (99% $^{13}$C; Cambridge Isotope Laboratories, Andover, U.S.A.) with ambient salinity (30‰) to obtain a final concentration of 1 g $^{13}$C m$^{-2}$ (Middelburg et al. 2000).

The sediment was sampled 2 h and 4 h after label addition during the first low tide (the pulse-labeling period) and subsequently at 12 h, 1 d, 2 d, 3 d, and 5 d exactly at low tide (the chase period). At each sampling time, approximately 5 mL pore-water was collected with porous polymer sippers (Rhizon Soil Moisture Sampler; Eijkelkamp Agrisearch Equipment) inserted into the upper 15 mm of the sediment and mixed from two randomly chosen positions within the sampling grid of each frame. One milliliter of the mixed pore-water sample per frame was dispensed into airtight headspace vials and analyzed for $^{13}$C-DIC (dissolved inorganic carbon) and the remainder was used for inorganic nutrient analysis. Water column nutrient data are from the NIOZ monitoring program from a station 500 m away from the diatom mat that was sampled every month.

Sediment samples were collected and mixed from the two randomly chosen positions within the sampling grid of each frame. Sediment was collected by pushing a core liner (inside diameter 100 mm) into the sediment to a depth of 50 mm and subsequently the top 15 mm of the sediment was sampled with a spatula (Middelburg et al. 2000). The sampling hole was filled with unlabeled sediment collected just outside the sampling frames and the core liner was removed. The two sediment samples taken from each frame were homogenized and subsampled for the different analyses. Samples for total organic carbon (TOC), CHO, AA, and FA were directly frozen in liquid nitrogen and subsequently lyophilized and stored at −20°C prior to analysis. Samples for pigments and nucleic acids were also frozen in liquid nitrogen and were stored at −80°C prior to analysis. Sediment samples for extracellular polymeric substances (EPS) were extracted within 30 min after sampling as described in Miyatake et al. (2014). Two operationally defined EPS fractions were distinguished: EPS extracted by Milli-Q (Millipore Cooperation) purified water (MQ) and EPS extracted by EDTA (de Brouwer and Stal 2001).

A miniaturized pulse amplitude modulated fluorimeter (Mini-PAM, Walz GmbH, Effeltrich, Germany) was used to monitor photosynthetic parameters. Intact sediment cores (100 mm cross-section and 250 mm deep) of the diatom mat

were taken in duplicate. Rapid light curves (RLCs) were recorded in the field at ambient conditions simultaneously with the pulse-labeling period. Prior to recording RLCs, samples were dark-adapted for 15 min to relax non-photochemical quenching. Subsequently, RLCs were recorded with 12 incremental irradiance steps of 20 s. From these data, the relative maximum photosynthetic electron transport rate, the light affinity coefficient (alpha), and the light saturation irradiance were determined (Serôdio et al. 2005).

During the $^{13}C$ label incorporation and RLCs recordings PAR (400–700 nm) was measured on site every 15 min by a Li-cor light meter (LI-250A) connected to a quantum sensor (Li-cor, Lincoln, Nebraska, U.S.A.). Throughout the year, a PAR sensor (Licor, LI-191) connected to a data logger (Licor, LI-1000), located 10 km from the study area, measured PAR values every minute; data was averaged and logged hourly.

During winter (February) and summer (August) the species composition of the diatom mat was determined. Samples for diatom identification were taken in duplicate by scraping a few grams of sediment of the surface to a depth of 5 mm. Subsequently, the sample was fixed in 1% glutaraldehyde/formaldehyde (volume ratio 1 : 10) in artificial seawater (30‰) and stored at 4°C. For diatom identification, frustules were cleaned by concentrated hydrogen peroxide oxidation and about 200 valves per sample were identified by light microscopy (Sabbe et al. 1995). Relative cell numbers were converted into relative contributions to total biovolume using the equations of Hillebrand et al. (1999). Taxa were divided into three growth forms, i.e., epipelic (motile), epipsammic (non-motile) and tychoplanktonic (*see* Barnett et al. 2015 for more details).

**Analytical procedures**

The carbon content and isotopic composition of TOC were analyzed by elemental analyzer/isotope ratio mass spectrometer (EA/IRMS) after the removal of carbonate with hydrochloric acid (Boschker et al. 1999). For DIC analysis, pore-water samples were acidified by adding 0.1 mL of 19 mol $L^{-1}$ phosphoric acid (Miyajima et al. 1995) and headspace gas was injected into an EA/IRMS in order to determine the concentration and isotopic composition of DIC.

Carbon content and isotopic composition of CHOs, AAs and nucleic acids in bulk sediment were analyzed by LC/IRMS. Likewise, EPS was analyzed by LC/IRMS for CHO carbon content and isotopic composition. For CHOs, 500 mg freeze dried sediment and 4 mL MQ EPS and EDTA EPS extracts were hydrolyzed to monosaccharides under acidic conditions using a modified method according to Cowie and Hedges (1984). Instead of neutralizing the hydrolysates with barium carbonate, the samples were neutralized with strontium carbonate, which resulted in an increase yield of the extract. EDTA was removed from the EDTA EPS hydrolysate as described in Moerdijk-Poortvliet et al. (2014*a*) and samples were analyzed by LC/IRMS as described in Boschker et al. (2008). For AAs, 700 mg freeze dried sediment was hydrolyzed with 6 M HCl for 20 h at 110°C and subsequently purified by cation-exchange chromatography (Veuger et al. 2005) and analyzed by LC/IRMS as described in McCullagh et al. (2006). For nucleic acids, desoxyribonucleic acid (DNA) and ribonucleic acid (RNA) were co-extracted from fresh sediment samples (5–10 g), enzymatically hydrolyzed to 5′-mononucleotides and analyzed by LC/IRMS as described in Moerdijk-Poortvliet et al. (2014*b*). Liquid chromatography was carried out using a Surveyor liquid chromatograph connected to an LC Isolink interface and a Delta V Advantage IRMS (all from Thermo Fisher, Bremen, Germany).

Lipids were extracted from 4 g dry weight of sediment with a modified Bligh and Dyer extraction (Boschker et al. 1999). The lipid extract was fractionated on silicic acid (Merck 60) into different polarity classes by sequential eluting with chloroform, acetone, and methanol. The chloroform fraction contained mainly neutral lipid-derived FA (NL), while the acetone and methanol fraction contained polar lipids-derived FA (i.e., mainly glycolipids-derived FA and phospho-lipids-derived FA respectively, but both fractions also contained other lipids such as betaine lipids and sulfolipids) (Heinzelmann et al. 2014). The acetone and the methanol fraction were denoted as respectively polar lipid 1 (PL1) and polar lipid 2 (PL2). All fractions were converted into FA methyl esters and the carbon content and isotopic composition of these derivatives were measured by GC/IRMS (Middelburg et al. 2000).

Pigments were extracted with acetone (90%, buffered with 5% ammonium acetate) from freeze-dried sediment, and analyzed by reverse-phase high-performance liquid chromatography (Dijkman and Kromkamp 2006).

Nutrient concentrations in pore-water samples were analyzed using a segmented continuous flow analyzer (SEAL QuAAtro XY-2 autoanalyzer, Bran and Luebbe, Norderstedt, Germany), according to the instructions provided by the manufacturer.

**Data analyses**

Benthic diatom biomass (expressed as mmol C $m^{-2}$) was calculated from the difference between total PL 2 and the bacteria-specific PL 2 pool (i.e., i14:0, i15:0, a15:0, i16:0, and 18:1$\omega$7c), as benthic diatom biomass = $(\Sigma PL2_{total} - \Sigma PL2_{bacteria})/a$, where a is the average PL2 concentration in benthic diatoms (0.053 mmol of C PL2 per mmol biomass benthic diatoms) (Evrard et al. 2008). Alternatively, benthic diatom biomass was calculated from chlorophyll *a* (Chl *a*) content assuming a carbon to Chl *a* ratio of 40 (de Jonge 1980; Middelburg et al. 2000).

In order to provide insight and overview of obtained data carbon pools were divided into storage and structural compounds. Storage carbon pools were defined as the sum of glucose and NL. Structural carbon pools were defined as the

**Table 1.** Explanatory and production parameter notation.

| Explanatory variables | | Production parameters | |
|---|---|---|---|
| **PAR** | Photosynthetic active radiation | | *Carbohydrates* |
| **Tsed** | Sediment temperature | **GLC** | Glucose; storage carbohydrate |
| | | **CHOstruct** | Structural carbohydrates |
| *Photosynthetic Parameters* | | **EPS** | Extracellular polymeric substances |
| **ETRMax** | Maximum electron transport rate | *Amino acids* | |
| α | Light affinity coefficient | **AA-1N** | Amino acids containing 1 N atom |
| **Ek** | Light saturation irradiance | **Lys-2N** | Amino acids containing 2 N atoms |
| *Pigments* | | **His-3N** | Amino acids containing 3 N atoms |
| **β-CARO** | $\beta$-carotene | **Arg-4N** | Amino acids containing 4 N atoms |
| **CLA** | Chl *a* | *Neutral lipid-derived fatty acids* | |
| **CLC** | Chl *c* | **NL-SFA** | Neutral lipid-derived saturated fatty acids |
| **DIAD** | Diadinoxanthin | **NL-MUFA** | Neutral lipid-derived mono unsaturated fatty acids |
| **DIAT** | Diatoxanthin | **NL-PUFA** | Neutral lipid-derived poly unsaturated fatty acids |
| **PHOR** | Pheophorbide | *Polar lipid-derived fatty acids* | |
| **FUCO** | Fucoxanthin | **PL1-SFA** | Polar lipid 1-derived saturated fatty acids |
| **PHYT** | Pheophytin | **PL1-MUFA** | Polar lipid 2-derived poly unsaturated fatty acids |
| *Nutrients* | | **PL1-PUFA** | Polar lipid 1-derived poly unsaturated fatty acids |
| **w-NH4** | Water column ammonium | **PL2-SFA** | Polar lipid 2-derived saturated fatty acids |
| **w-NO2** | Water column nitrite | **PL2-MUFA** | Polar lipid 2-derived mono unsaturated fatty acids |
| **w-NO3** | Water column nitrate | **PL2-PUFA** | Polar lipid 2-derived poly unsaturated fatty acids |
| **w-PO4** | Water column phosphate | *Nucleic acids* | |
| **w-Si** | Water column silicate | **DNA** | Desoxyribonucleic acid |
| **pw-NH4** | Pore water ammonium | **RNA** | Ribonucleic acid |
| **pw-NO2** | Pore water nitrite | | |
| **pw-NO3** | Pore water nitrate | | |
| **pw-PO4** | Pore water phosphate | | |
| **pw-Si** | Pore water silicate | | |

sum of structural CHOs (CHO structural, i.e., fucose, rhamnose, galactose, mannose, and xylose), PL 1, PL 2, AA, DNA, and RNA. AAs were further divided into subgroups based on the number of nitrogen atoms in these compounds (i.e., AAs containing one nitrogen atom (AA-1N): aspartine (aps), hydroxyproline (hyp), serine (ser), threonine (thr), glutamine (glu), glycine (gly), alanine (ala), proline (pro), valine (val), methionine (met), isoleucine (ile), leucine (leu), tyrosine (tyr), and phenylalanine (phe); one AA containing two nitrogen atoms (AA-2N): lysine (lys); one AA containing three nitrogen atoms (AA-3N): histine (his) and one AA containing four nitrogen atoms (AA-4N): arginine (arg)) and the three polarity classes of FAs (i.e., NL, PL1, and PL2) into saturated FAs (SFA), mono-unsaturated FAs (MUFA) and poly-unsaturated FAs (PUFA). The data of the two operationally defined EPS fractions, analyzed for CHOs, were combined and referred to as EPS.

For the carbon pool production measurements, the absolute amount of $^{13}C$ incorporated into different carbon pools over the background was calculated. This value is expressed as excess $^{13}C$ and is calculated from $\delta^{13}C$ sample as:

$$\text{Excess } {}^{13}\text{C (mol } {}^{13}\text{C m}^{-2}) = \left[\left(\frac{(\delta^{13}C_{sample}/1000+1)\times R_{st}}{(\delta^{13}C_{sample}/1000+1)\times R_{st}+1}\right)\right] - \left[\left(\frac{(\delta^{13}C_{background}/1000+1)\times R_{st}}{(\delta^{13}C_{background}/1000+1)\times R_{st}+1}\right)\right] \times C_{sample}$$

where $\delta^{13}C_{background}$ denotes the $\delta^{13}C$ value of the unlabeled sample, $C_{sample}$ denotes the pool size in mol of carbon per square meter sediment (mol C $m^{-2}$), and $R_{st}$ denotes the $^{13}C/^{12}C$ ratio of the international standard Vienna Pee Dee Belemnite ($R_{st} = 0.0112372$). Carbon fixation rates of various carbon pools of the diatom mat were quantified by calculating the regression slope from sample data (at 0 h, 2 h, and 4 h) (expressed in $\mu$mol $^{13}C$ $m^{-2}$ $h^{-1}$).

The relative photosynthetic electron transport rate (rETR) was calculated by multiplying the Mini PAM measured quantum yield (i.e., "efficiency" of photosynthesis) and the applied irradiance (E) during the recording of the RLCs (Kromkamp and Forster 2003). From the RLCs the relative maximum photosynthetic electron transport rate ($ETR_{max}$), the light affinity coefficient in the light limited region of the

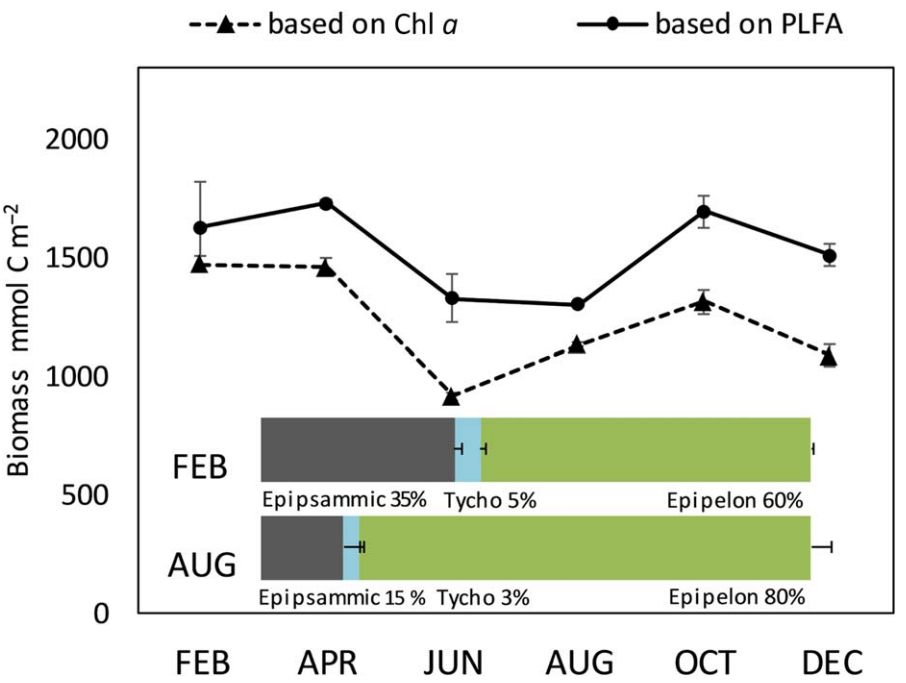


**Fig. 2.** Diatom biomass based on respectively Chl *a* and PL2-derived FA (assumed to be mainly phospholipid-derived fatty acids [PLFA]). Months are from the year 2011. Bars denote winter and summer community composition of the diatom mat. Error bars: standard deviation ($n = 2$).

RLC (alpha), and the light saturating irradiance ($E_k$ = ETR$_{max}$/alpha) were determined by fitting the RLCs to a modified version of the equation of Eilers and Peeters (1988): rETR $= E/aE^2 + bE + c$), where $a = (\text{alpha} \times E_k^2)^{-1} - 2 \times (\text{alpha} \times E_k)^{-1}$; $c = \text{alpha}^{-1}$.

The relationship between production rates of the various carbon pools and environmental, photosynthetic, and pigment parameters (i.e., explanatory variables) were analyzed by Co-Inertia Analysis (Dolédec and Chessel 1994); this data table coupling technique is especially adapted to tables composed of a relatively high number of variables (Dray et al. 2003) as in our study. Production and explanatory data were processed by normalized Principal Component Analysis (PCA). These two PCAs were then combined in a Co-Inertia Analysis (CoIA) in order to highlight the common information between explanatory and production measurements (Dolédec and Chessel 1994; Dray et al. 2003). The correlation between the explanatory and production data set was assessed by the *Rv* coefficient (Escoufier 1973) and its significance was tested by a randomization procedure of 9999 permutations of table lines (Heo and Gabriel 1998). Similarly, the $^{13}C$ excess data table of the various carbon pools after 3 d was also processed by a normalized PCA and its relationship with explanatory variables were analyzed by Co-Inertia Analysis. The notation of the various parameters is explained in Table 1. Time-point "day 3" was chosen, because from that time-point on label distributions remained relatively similar. Multivariate analyses and associated graphical representations were run with "ade4" package (Chessel et al. 2004) in R version 3.2.3 (R Development Core Team 2015).

## Results

### Seasonal development of the diatom mat

Benthic diatoms were visible on the sediment surface during the whole year but varied in density, depending on the time of the year and the time of the day. Trends in benthic diatom biomass estimated from Chl *a* and FAs biomarker data were in good agreement (Fig. 2).

The benthic diatom biomass was highest in winter and lowest during June and August (Fig. 2). The decrease in biomass coincided with the activity of bioturbating fauna that grazed the diatom mat (observed visually). The species composition of the diatom mat was determined in winter (February) and summer (August). On average $40 \pm 3$ different diatom species were observed. In terms of biovolume, epipelic diatoms dominated the community in both months and the proportion of epipsammic diatoms was highest in February. The proportion of tychoplanktonic diatoms was always low (Fig. 2). Epipelic diatoms were dominated by *Entomoneis* sp. (comprising 47 and 35 biovolume (BV) % of this group in winter and summer, respectively), tychoplanktonic diatoms were dominated by *Cymatosira belgica* (comprised respectively 49 BV % and 65 BV % of this group in winter and summer, respectively), and epipsammic diatoms by *Dimeregramma minor* (comprised respectively 46 BV % and 61 BV % of this group in winter and summer, respectively). Diatom community composition of the mats is presented in Table 2.

The observed pigment profiles during the year were typical for diatoms, including *β*-carotene, Chl *a*, Chl *c*,

**Table 2.** Community composition of the diatom mat in respectively winter (February) and summer (August). Biovolumes are based on Hillebrand et al. (1999).

| | | Abundance | | | |
|---|---|---|---|---|---|
| | | Feb | | Aug | |
| Species | Biovolume $\mu m^3$ | % | SD* | % | SD* |
| **Epipsammic species** | | | | | |
| *Dimeregramma minor* | 251 | 16.3 | 3.6 | 9.3 | 2.0 |
| *Pseudostaurosira perminuta* | 98 | 5.9 | 0.8 | 1.1 | 0.2 |
| *Plagiogramma staurophorum* | 467 | 2.8 | 2.8 | 1.2 | 0.3 |
| *Opephora mutabilis* | 92 | 2.4 | 0.1 | 0.5 | 0.2 |
| *Planothidium delicatulum* | 184 | 2.3 | 0.7 | 0.9 | 0.5 |
| *Cocconeis peltoides* | 377 | 1.9 | 0.9 | 1.3 | 0.1 |
| *Cocconeis* sp. | 244 | 1.1 | 0.5 | 0.1 | 0.1 |
| *Opephora guenter-grassii* | 47 | 0.9 | 0.1 | 0.1 | 0.0 |
| *Catenula adhaerens* | 81 | 0.7 | 0.3 | 0.2 | 0.0 |
| *Fragilaria* cf. *subsalina* | 82 | 0.4 | 0.0 | 0.0 | 0.0 |
| *Fallacia aequorea* | 66 | 0.2 | 0.1 | 0.1 | 0.1 |
| *Cocconeis placentula* | 57 | 0.2 | 0.0 | 0.2 | 0.1 |
| *Amphora pediculus* | 176 | 0.1 | 0.1 | 0.0 | 0.0 |
| *Fallacia cryptolyra* | 77 | 0.1 | 0.1 | 0.1 | 0.1 |
| *Achnanthes amoena* | 91 | 0.1 | 0.1 | 0.0 | 0.0 |
| **Total epipsammic species** | | **35** | **2** | **15** | **3** |
| **Tychoplanktonic species** | | | | | |
| *Cymatosira belgica* | 189 | 2.3 | 0.3 | 1.8 | 1.0 |
| *Thalassiosira decipiens* | 1105 | 1.6 | 0.0 | 0.8 | 0.1 |
| *Plagiogrammopsis vanheurckii* | 366 | 0.5 | 0.0 | 0.1 | 0.1 |
| *Delphineis minutissima* | 118 | 0.3 | 0.2 | 0.1 | 0.1 |
| **Total tychoplanktonic species** | | **5** | **1** | **3** | **1** |
| **Epipelic species** | | | | | |
| *Entomoneis* sp. | 9660 | 28.0 | 0.7 | 28.8 | 11.2 |
| *Navicula gregaria* | 1251 | 9.9 | 2.5 | 1.5 | 1.5 |
| *Tryblionella apiculata* | 1633 | 5.8 | 3.4 | 3.0 | 1.0 |
| *Staurophora salina* | 3535 | 5.3 | 0.0 | 12.7 | 2.0 |
| *Amphora* cf. *copulata* | 655 | 1.9 | 0.0 | 2.8 | 0.4 |
| *Navicula arenaria var. rostellata* | 2227 | 1.7 | 0.0 | 1.4 | 1.4 |
| *Amphora laevis var. laevissima* | 564 | 1.6 | 0.0 | 0.5 | 0.5 |
| *Amphora coffeaeformis* | 1837 | 1.3 | 1.3 | 3.0 | 1.5 |
| *Cosmioneis* sp. | 1251 | 0.9 | 0.9 | 0.0 | 0.0 |
| *Navicula phyllepta* | 451 | 0.7 | 0.0 | 4.1 | 0.3 |
| *Navicula* sp. 1 | 276 | 0.6 | 0.6 | 0.8 | 0.8 |
| *Navicula flanatica* | 679 | 0.5 | 0.5 | 0.0 | 0.0 |
| *Haslea* sp. | 679 | 0.5 | 0.5 | 0.0 | 0.0 |
| *Navicula perminuta* | 84 | 0.4 | 0.1 | 0.2 | 0.0 |
| *Seminavis* sp. | 524 | 0.4 | 0.4 | 0.2 | 0.2 |
| *Diploneis aestuarii* | 251 | 0.4 | 0.4 | 0.0 | 0.0 |
| *Navicula microdigitoradiata* | 432 | 0.3 | 0.3 | 2.3 | 0.2 |
| *Fallacia clamans* | 77 | 0.1 | 0.1 | 0.0 | 0.0 |
| *Incertae sedis 1* | 451 | 0.0 | 0.0 | 2.1 | 0.6 |
| *Nitzschia* cf. *dissipata* | 318 | 0.0 | 0.0 | 0.1 | 0.1 |
| *Fallacia pygmaea* | 2225 | 0.0 | 0.0 | 6.1 | 0.6 |

**TABLE 2.** Continued

| Species | Biovolume $\mu m^3$ | Abundance | | | |
|---|---|---|---|---|---|
| | | Feb | | Aug | |
| | | % | SD* | % | SD* |
| *Psammodictyon panduriforme var. delicatulum* | 596 | 0.0 | 0.0 | 0.2 | 0.2 |
| *Fallacia forcipata* | 1301 | 0.0 | 0.0 | 1.2 | 1.2 |
| *Amphora* sp. 2 | 180 | 0.0 | 0.0 | 0.4 | 0.1 |
| *Delphineis surirella* | 1131 | 0.0 | 0.0 | 0.3 | 0.3 |
| *Tryblionella coarctata* | 2969 | 0.0 | 0.0 | 0.9 | 0.9 |
| *Amphora lineolata* | 1837 | 0.0 | 0.0 | 1.1 | 1.1 |
| *Gyrosigma* sp. 3 | 8863 | 0.0 | 0.0 | 8.1 | 0.0 |
| *Amphora* sp. 1 | 564 | 0.0 | 0.0 | 0.2 | 0.2 |
| **Total epipelic species** | | **60** | **1** | **82** | **4** |

* SD, standard deviation ($n = 2$).

fucoxanthin, diadinoxanthin, and diatoxanthin (Supporting Information Table S1). The photosynthetic parameters Ek and ETRmax were higher in early spring and summer, while $\alpha$ was higher in autumn and winter (Supporting Information Table S1).

The analyzed carbon pools explained only 18% ± 1% of the TOC (Fig. 3). The distribution of the different carbon components was more or less the same throughout the year with 58% ± 3% CHOs, 25% ± 3% AAs, 16% ± 3% FAs, and 1% ± 0% nucleic acids (Table 3; Fig. 3).

**Pulse period: initial production of carbon pools**

The total carbon fixation and the production of the individual carbon pools during the first 4 h of the in situ labeling experiments showed a strong seasonal pattern. February and April were the most productive months and October and December the least productive (Fig. 4A). Of the total determined carbon pools production, the production of storage carbon (glucose and NL) was much more important than the production of structural carbon with respectively 81% ± 5% and 19% ± 1% (Table 3).

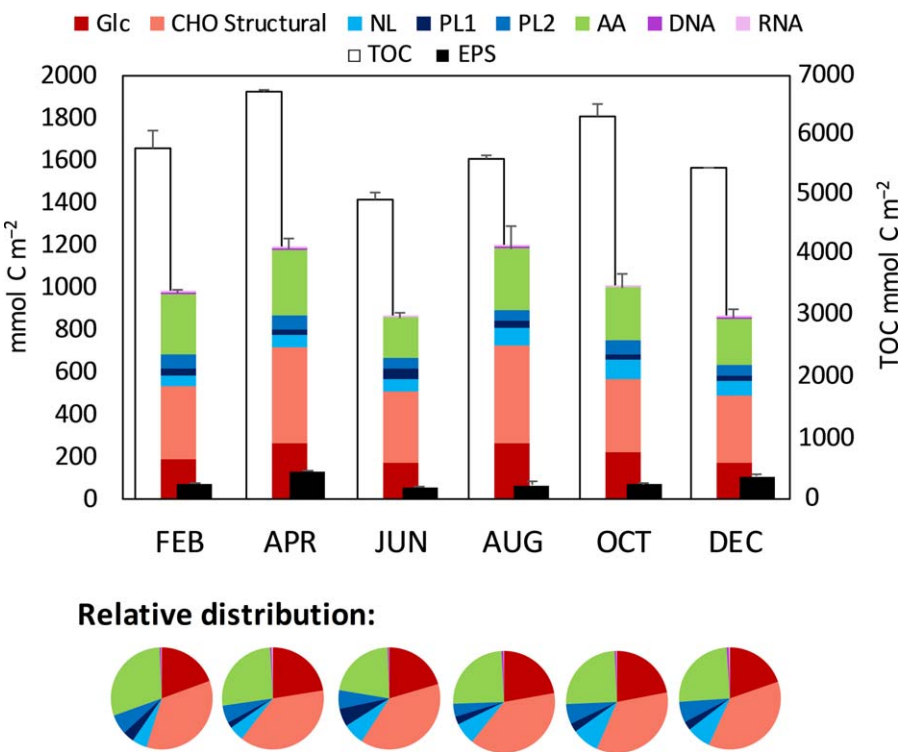


**Fig. 3.** Annual absolute and relative composition of the sediment organic matter. Presented concentrations are the average of all values obtained during the length of the experiments (i.e., 5 d). Error bars: standard deviation ($n = 2$).

**Table 3.** Composition of the sediment organic matter and production of individual carbon pools expressed as a percentage of the total carbon production.

| | Sediment organic matter (%) | Carbon production (%) | |
|---|---|---|---|
| Carbon pool | Annual | Other months* | Summer† |
| **Total carbon** | | | |
| Glc | 21 ± 1 | 72 ± 4 | 59 ± 6 |
| NL | 7 ± 2 | 9 ± 4 | 21 ± 0 |
| PL1 | 3 ± 1 | 2 ± 1 | 6 ± 3 |
| CHO structural | 37 ± 2 | 9 ± 2 | 10 ± 2 |
| PL2 | 6 ± 1 | 3 ± 2 | 4 ± 2 |
| AA | 25 ± 3 | 5 ± 2 | 3 ± 1 |
| DNA | 0.5 ± 0.1 | 0.01 ± 0.01 | 0.02 ± 0.001 |
| RNA | 0.3 ± 0.1 | 0.06 ± 0.03 | 0.05 ± 0.01 |
| **Storage carbon** | | | |
| Glc | 76 ± 4 | 88 ± 5 | 73 ± 2 |
| NL | 24 ± 4 | 12 ± 5 | 27 ± 2 |
| **Structural carbon** | | | |
| CHO | 51 ± 3 | 43 ± 17 | 47 ± 10 |
| AA | 35 ± 3 | 27 ± 6 | 14 ± 1 |
| PL1 | 5 ± 2 | 10 ± 4 | 24 ± 6 |
| PL2 | 7 ± 2 | 15 ± 6 | 16 ± 4 |
| DNA | 0.8 ± 0.3 | 0.08 ± 0.08 | 0.15 ± 0.05 |
| RNA | 0.2 ± 0.1 | 0.45 ± 0.19 | 0.28 ± 0.02 |
| **Excreted carbon** | | | |
| EPS | 10 ± 3 | 21 ± 6 | 9 ± 4 |
| **Nucleic acid C** | | | |
| DNA | 69 ± 8 | 14 ± 8 | 33 ± 6 |
| RNA | 31 ± 8 | 86 ± 8 | 67 ± 6 |

±, standard deviation ($n = 2$).
* February, April, October, December.
† June, August.

Glucose strongly dominated storage carbon production throughout the year. The $^{13}C$ label distribution in the analyzed carbon pools was similar in February, April, October, and December. In the summer months, the $^{13}C$ label distribution was different as NL became more important than in other seasons (27% ± 2% in summer vs. 12% ± 5% in other seasons; Table 3; Fig. 4A). For structural carbon, a relative low AA production was found in summer compared to other seasons respectively 14% ± 1% vs. 27% ± 6%. This is in contrast to the relatively higher PL1 production in summer (24% ± 6%) compared to other seasons (10% ± 4%) (Table 3). The RNA production was higher than DNA production, irrespective of the month of sampling. However, the DNA production was relatively more important in summer than in other seasons (33% ± 6% vs. 14% ± 8% of the total nucleic acids, Table 3; Fig. 4B). For the production of PL2 and the structural CHO, we did not observe a seasonal effect (Table 3). The percentage of fixed CHO excreted as EPS was lower in summer than in other months, which were 9% ± 4% and 21% ± 6%, respectively (Table 3). Therefore, the main seasonal differences were that during summer the diatom mat showed a higher production of DNA relative to RNA, a higher production of PL1-derived FAs, a larger part of the fixed carbon was redirected to storage lipids instead of glucose, and that the percentage of fixed CHO excreted as EPS was lower.

Substantial $^{13}C$ label was incorporated in the TOC pool during the initial 4 h labeling period (Fig. 4A). The analyzed carbon pools explained on average 55% ± 7% of the $^{13}C$ label incorporated in the TOC, however a substantial fraction (~ 45%) was therefore not accounted for (Fig. 4A). For most months, the maximum amount of incorporated $^{13}C$ label was reached at $t = 4$ h where after excess $^{13}C$ substrate was washed away due to immersion. However, in June $^{13}C$ bicarbonate label incorporation continued after $t = 4$ h and reached a maximum at $t = 12$ h (Fig. 5). Presumably, bioturbation of the sediment resulted in a deeper burial of the $^{13}C$ bicarbonate label and resulted in an increased label residence time in the pore-water. This, in combination with prolonged day lengths, might be the cause of the ongoing label incorporation between $t = 4$ h and $t = 12$ h.

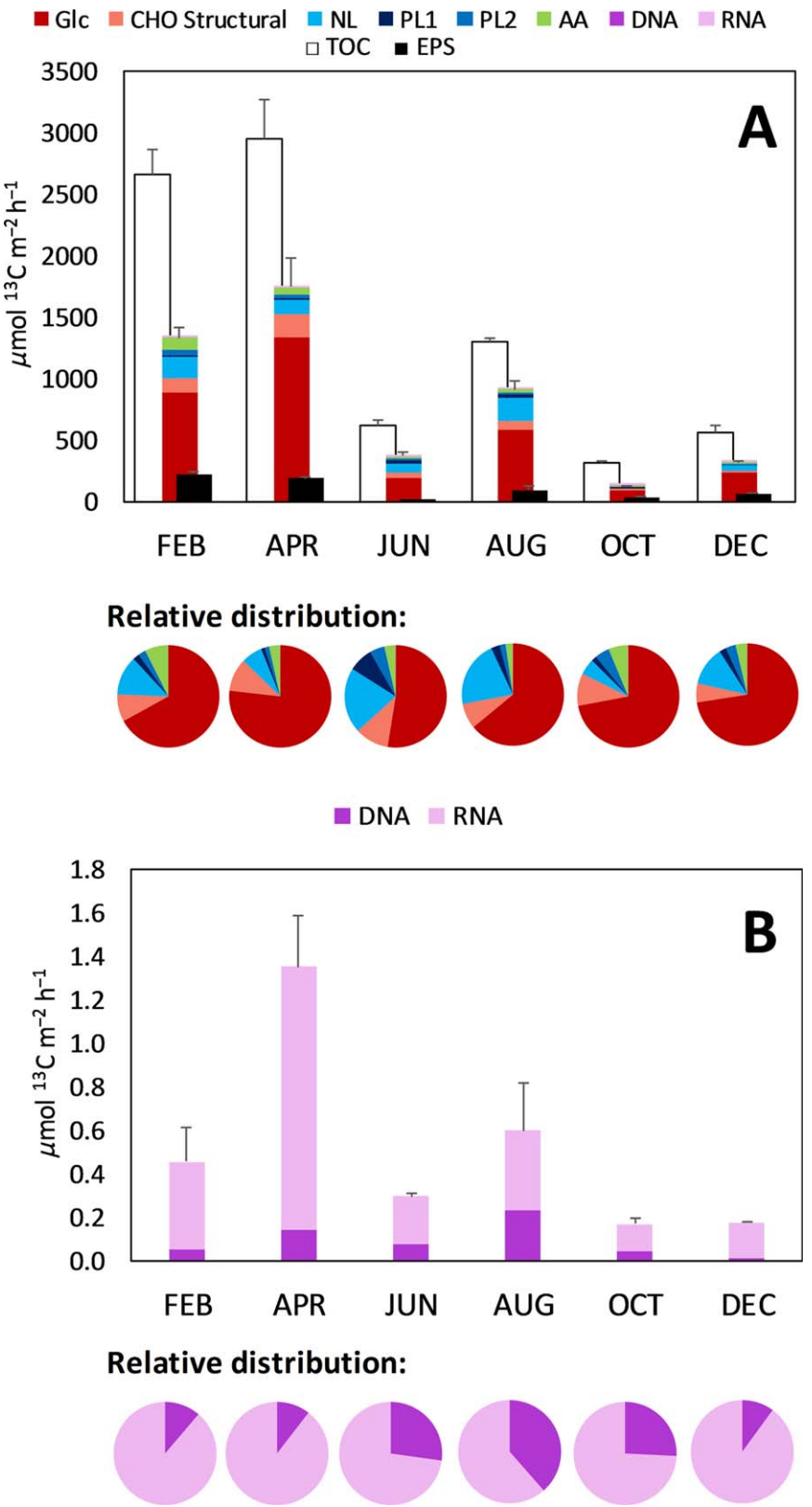


**Fig. 4.** Annual absolute and relative distribution of determined carbon production rates (**A**) and DNA and RNA production rates of the diatom mat (**B**). Error bars: standard deviation ($n = 2$).

**Chase period: loss and redistribution of incorporated $^{13}C$ label**

By studying the chase period (12 h to 5 d) we gained insight in the dynamics of the various produced carbon pools after bicarbonate label was washed away by the tides (Fig. 5). On average only 1.7% ± 0.9% of the initially applied $^{13}C$-DIC remained in the sediment pore-water after 12 h of the start of experiment, confirming that most of it was washed away (or exchanged with the atmosphere). Both storage carbon in the form of glucose and neutral lipids, and EPS showed a steep decrease in $^{13}C$ labeling during the first 20 h of the chase period (Figs. 5 and 6A1–F1). Most structural compounds like AA, structural CHO, PL1, and PL2 showed a more gradual loss of $^{13}C$ label (Fig. 6A2–F2), while the DNA and RNA pools showed hardly any label loss, but instead increased labeling during the course of the experiment, in particular in DNA (Fig. 6A3–F3). The main difference between storage and structural compounds was that the turnover of storage compounds was fast whereas the turnover of structural compounds, especially in the case of DNA and RNA, was slow.

Net label loss was studied by comparing the amount of incorporated $^{13}C$ label at $t = 4$ h with the $^{13}C$ label remainder after 3 d. For both storage and structural carbon, the highest loss of incorporated $^{13}C$ label was observed in the months February and April (respectively 89% ± 2% and 48% ± 8%, Fig. 6A1,A2,6B1,B2) while in the other seasons it was lower (respectively 76% ± 3% and 9% ± 14%, Fig. 6C1–F1,6C2–F2). Throughout the year, glucose accounted for most of the loss of $^{13}C$ label of storage compounds (86% ± 12%) but in summer also NL contributed substantially to this loss (27% ± 2%). Throughout the year, the loss of structural carbon was mainly attributed to the loss of $^{13}C$ label from the structural CHO and AA pools, while the $^{13}C$ label content in other structural pools, such as PL1 and PL2, moderately decreased or remained constant (Fig. 6A2–F2).

It should be noted that the percentage of TOC explained by the $^{13}C$ label incorporated in the biochemical carbon pools decreased from 55% ± 7% at $t = 4$ h to 33% ± 10% at day 3 (Fig. 5). This suggested transfer of a substantial amount of label to an unknown carbon pool within the TOC. The label transfer to the unknown carbon pool was lowest during summer (15% ± 3% compared to 27% ± 3% during the rest of the year).

**Environmental parameters**

Pore-water nutrient concentrations were always higher than nutrient concentrations in the water column above the sediment (during immersion) (Supporting Information Table S1). Inorganic nitrogen was predominantly present as ammonium in the pore water and nitrate in the overlying water. Average pore water inorganic nitrogen concentrations were lower in summer (June and August) compared to the rest of the year (respectively 27.9 ± 0.1 $\mu$mol $L^{-1}$ and 72 ± 27 $\mu$mol $L^{-1}$). N:P ratios above Redfield (i.e., 16) were observed from February until June (26 ± 5). In August and October N:P ratios were below Redfield (7 ± 1) and in December near Redfield (17 ± 1) (Supporting Information Table S1). Likewise, inorganic nitrogen concentrations in the overlying water were lower in summer (June and August) compared to the rest of the year (respectively 14 ± 3 $\mu$mol $L^{-1}$ and 38 ± 16 $\mu$mol $L^{-1}$). The seasonal trend of nutrient N:P ratios in the overlying water was similar as in the pore water and were above Redfield from February until June and in December (46 ± 30) and below Redfield in August and October (12 ± 2) (Supporting Information Table S1). The exact nutrient concentrations in the thin diatom mat could not be determined and are therefore unknown. The concentration of organic nutrients like urea was not measured. PAR values correlated to sediment temperatures and were higher in summer than in winter. The average temperature and daily integrated photon irradiance during the 4 h of $^{13}C$ labeling of the diatom mat were the lowest in February (3.7°C and 1314 $\mu$mol photons $m^{-2}$ and the highest in August (20.5°C and 7492 $\mu$mol photons $m^{-2}$) (Supporting Information Table S1).

**Co-inertia analysis**

Co-Inertia Analysis was done on the$^{13}C$ labeling data set and on explanatory variables (environmental, pigments, and photosynthetic parameters) at the end of the pulse period (4 h) (Fig. 7A,C,E) and at day 3 (Fig. 7B,D,F).

At the end of the pulse period (4 h) Co-Inertia Analysis revealed a strong and highly significant co-structure between the PCAs of the initial label incorporation (4 h) and explanatory variables ($Rv = 0.56$; $p = 0.004$). Two main axes summarized the variance common to both data sets (the duplicate datasets A and B, representing the two frames) (bar diagram Fig. 7A); both axes determined 92% of the variances of initial label incorporation and explanatory variables. The third axis is not discussed since it represented a basic thermal gradient accounting for only a small part of the variance. The two first axes expressed the major dynamics among three seasonal clusters.

The first axis opposed high productivity months (February and April) to lower productivity months (June, August, October, and December), whereas the second axis opposed summer/spring (April, June, and August) to winter/autumn (February, October, and December) (Fig. 7A). The February/April cluster had the highest synthesis rates of all determined carbon pools, except those of Arg-4N, DNA, PL1-MUFA, NL-MUFA, PL1-SFA, and NL-SFA. These latter groups were more or less independent of the first axis and characterized the highest synthesis rates in June/August in opposition to the low synthesis rates in October/December along the second axis (Fig. 7A,E). The highest synthesis rates encountered in February/April were consistently associated to high concentrations of light harvesting pigments, a well-

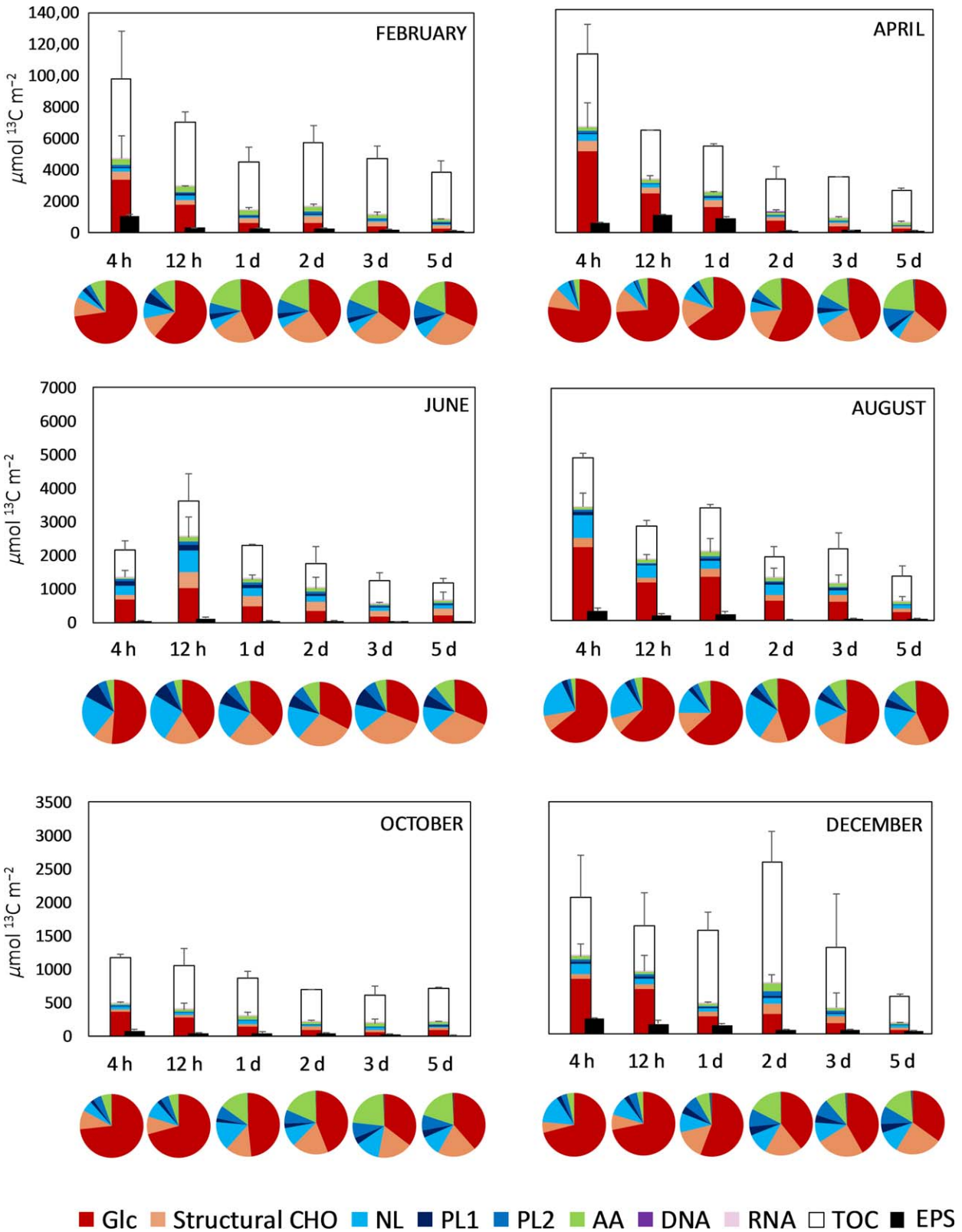


**Fig. 5.** Seasonal dynamics of $^{13}C$ label content and relative$^{13}C$ label distribution of all analyzed carbon pools during the label chase-period of the experiment. Error bars: standard deviation ($n = 2$).

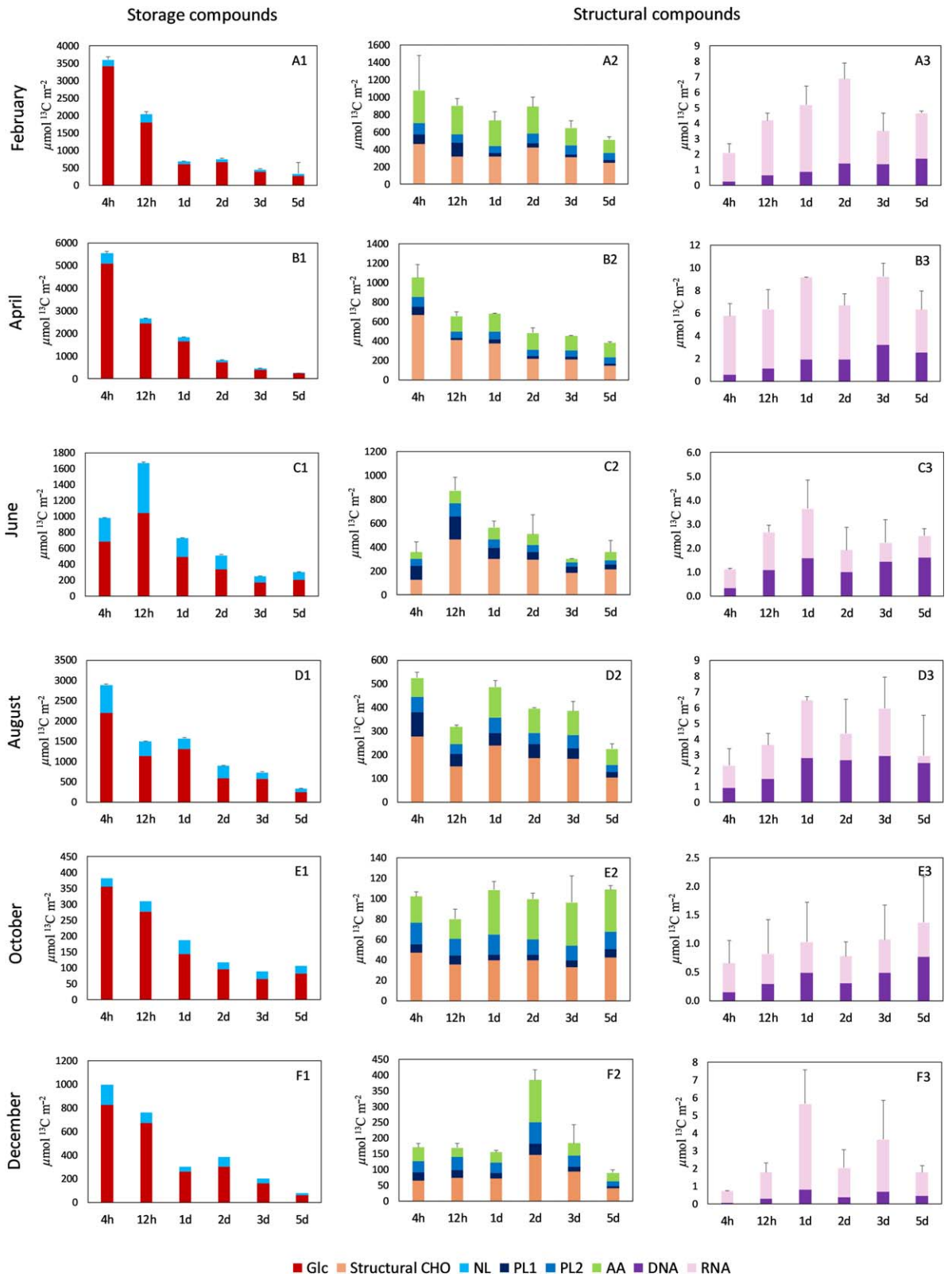


**Fig. 6.** Seasonal dynamics of $^{13}C$ label content of storage and structural carbon pools during the label chase-period of the experiment. Error bars: standard deviation ($n = 2$). Data for February, April, June, August, October and December (panels A, B, C, D, E, and F, respectively). Panels 1: storage carbohydrate (red, Glc) and neutral lipids (light blue, NL); panels 2: structural carbohydrate (orange, structural CHO), polar lipid 1 (black, PL1, acetone fraction), polar lipid 2 (dark blue, PL2, methanol fraction), and amino acids (green, AA); panels 3: nucleic acids DNA (dark purple) and RNA (light purple).

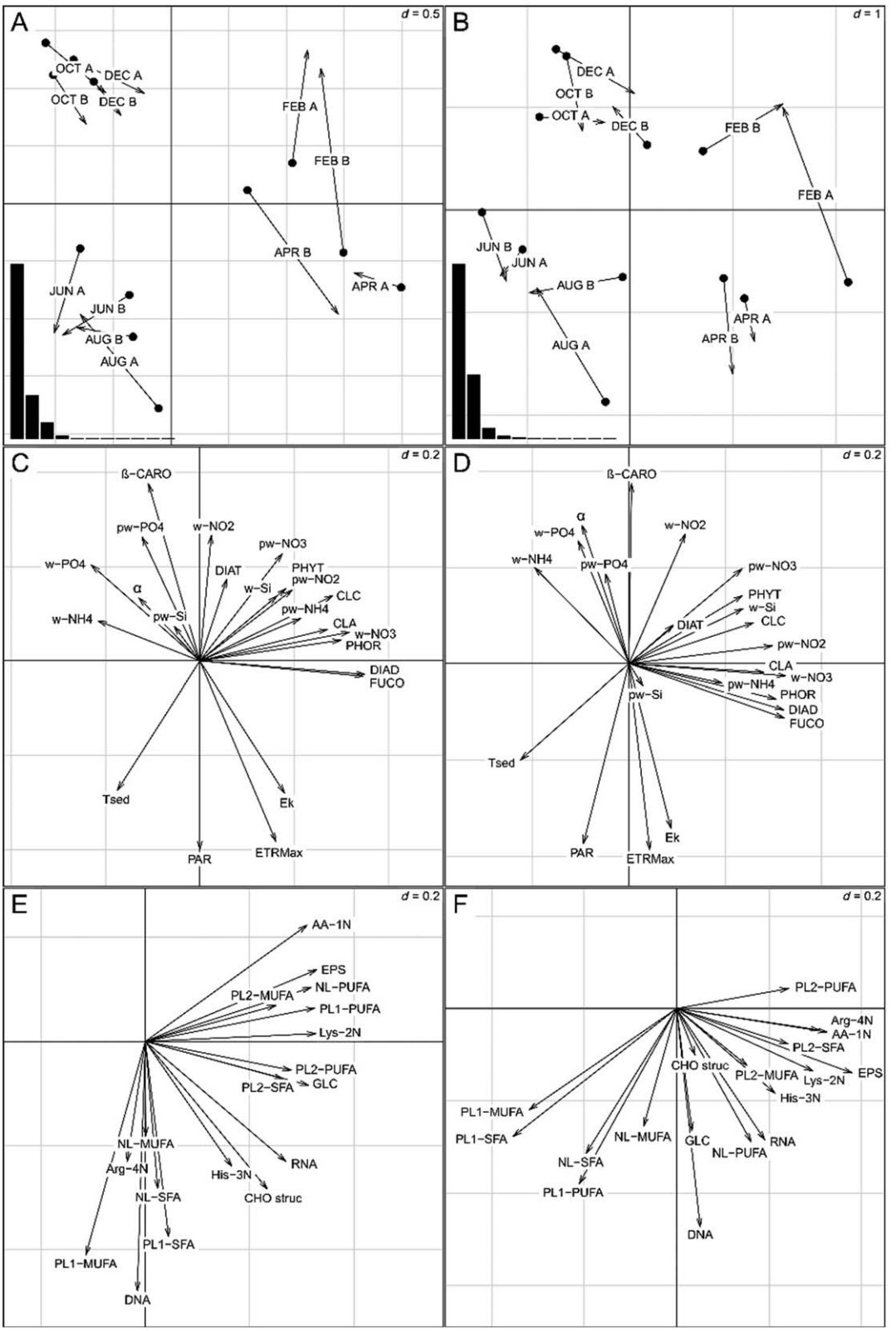


**Fig. 7.** Results of the co-inertia analysis. (**A**), (**C**), and (**E**) depict the relationships between $^{13}C$ label incorporation and explanatory variables) at 4 h (pulse period). (**B**), (**D**), and (**F**), depict the relationships between $^{13}C$ label content and explanatory variables at day 3 (chase period). (**A**) Co-structure between the patterns of production (black dots) and explanatory variables (arrow tip). Arrow length indicates the lack of fitting (short arrows indicate strong matching between the two data sets, similar to residuals in a regression). Pearson's correlation coefficients between the coordinates (black dot vs. their respective arrow tip) on the first axis: $r = 0.89$, $p < 0.001$ and on the second axis: $r = 0.73$, $p = 0.007$. (**B**. As 'A' but at day 3. Pearson's correlation coefficients between the coordinates (black dot vs. their respective arrow tip) on the first axis: $r = 0.85$, $p < 0.001$ and on the second axis: $r = 0.72$, $p = 0.008$. Eigenvalue diagrams (bars represent axis variances): (**A**) axis 1 (horizontal) and axis 2 (vertical), 74% and 18% respectively; (**B**) axis 1 (horizontal) and axis 2 (vertical), 69% and 25% respectively. (**C**) and (**E**), explanatory variables. (**D**) and (**F**), production and day 3 variables, respectively. "d" indicates the grid scale. The notation of the various parameters is explained in Table 1.

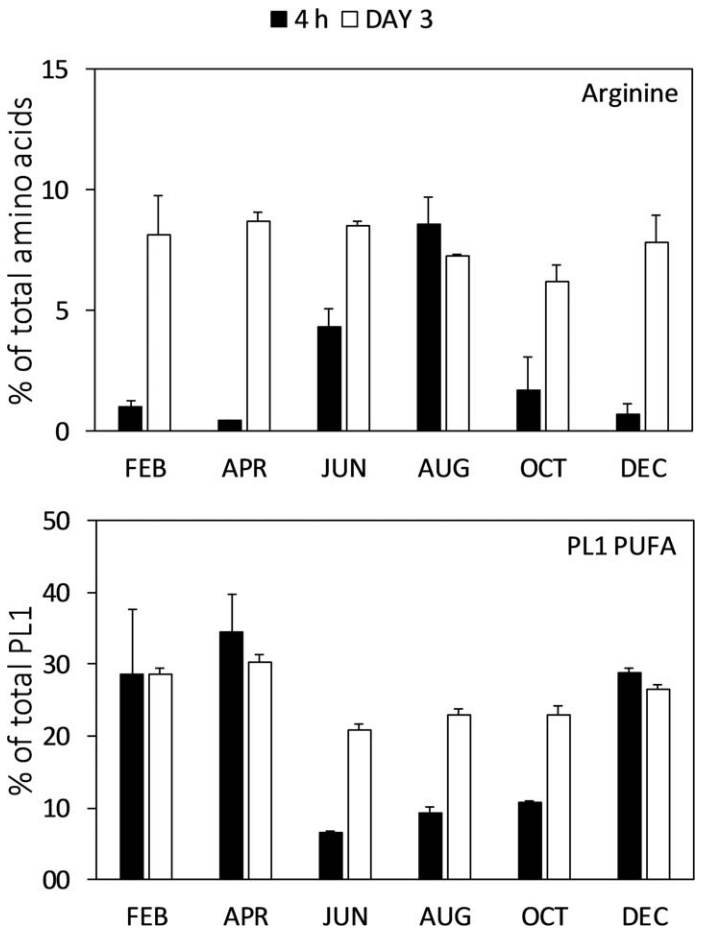


**Fig. 8.** Relative arginine and PL1-PUFA $^{13}C$ label incorporation at respectively $t = 4$ h and $t =$ day3. Both arginine and PL1-PUFA dynamics were different in summer compared to other seasons. Error bars: standard deviation ($n = 2$).

functioning photosynthetic apparatus (higher Ek and ETRmax), and higher inorganic nutrient contents. The second axis was strongly positively related to temperature and PAR, ETRmax and Ek, and negatively from June/August to October/December with alpha (i.e., the photosynthetic parameter for affinity to light), $\beta$-carotene content, phosphate concentrations and ammonium concentration in the overlying water (Fig. 7C).

The second Co-Inertia Analysis was done between the $^{13}C$ labeling data at day 3, when label distribution had more or less stabilized, and explanatory variables, and was also significant ($Rv = 0.53$; $p = 0.009$) (Fig. 7B,D,F). The two first Co-Inertia axes explained 91% and 95% of the variances of day 3 compounds and explanatory variables, respectively. The general pattern after 3 d was similar to the 4 h analysis, except for arginine and PL1-PUFA (compare Fig. 7B,D,F with Fig. 7A,C,E). Although the trends of arginine and PL1-PUFA remained more or less independent in both data sets, their positions swapped between the first ($t = 4$ h; Fig. 7E) to the second analysis ($t = 3$ d; Fig. 7F). Complementary, and in contrast with other compounds, arginine and PL1-PUFA $^{13}C$ loss dynamics during summer was different from that during the other seasons. Figure 8 shows that more $^{13}C$ label was found in arginine in summer and suggested a fast production followed by limited turnover, whereas during the other months, arginine production continued until day 3. PL1-PUFA showed a reverse trend compared to arginine (Fig. 8; Supporting Information Tables S2,S3). Most of the interpreted variables were significantly correlated to the co-inertia axes (Supporting Information Table S4).

## Discussion

In this in situ study the carbon flow within a benthic diatom mat was investigated by following the $^{13}C$-labeling dynamics in various cellular compounds. At regular intervals of 2 months during 1 yr, the fate of carbon fixation was followed and related to a number of environmental and photosynthetic parameters. The high isotopic enrichment of glucose indicated that the majority of photosynthetically fixed carbon was initially invested into intracellular chrysolaminaran and to a lesser extent into storage lipids, which also gained substantial label, especially during summer. The incorporated $^{13}C$ label in storage compounds disappeared quickly and was partially used for the production of structural cell material. Our data suggest however that most of the incorporated $^{13}C$ label was lost, either directly through diatom respiration or through EPS secretion followed by EPS loss to the overlying water or degradation by bacteria (Goto et al. 2001; Hanlon et al. 2006). Unfortunately, due to the design of the in situ experiments loss processes such as respiration and exchange with the overlying water could neither be determined nor distinguished. The strong initial enrichment of carbon-rich storage compounds in combination with the low labeling of structural compounds suggested that the dense diatom mat was unable to acquire enough nutrients for the synthesis of N or P containing structural cell material during the period of photosynthesis and, hence, that the fixed carbon was mainly stored as reserve material or excreted as EPS. It appeared that the transport of nutrients in the dense diatom mat was diffusion-limited resulting in a lower production of structural compounds (Stewart 2003). However, benthic diatoms were able to produce structural compounds such as DNA and RNA during the chase period. The nutrients required for the synthesis of these nucleic acids may have come from the overlying water during immersion or the diatoms may have migrated into the sediment where nutrients are available in higher concentrations. Hence, photosynthesis and the synthesis of structural cell components in the diatom mat were temporally separated (Mitbavkar and Anil 2004; Underwood et al. 2005). Since the production of non-nitrogenous CHOs predominated in all seasons we expect a high C:N ratio of the diatom mat

leading to a low nutritional value of the diatom mat for higher trophic levels (Brown et al. 1997; Jones and Flynn 2005) .

The diatom mat partitioned the fixed carbon between the measured carbon pools in a way that was remarkably different in summer compared to the rest of the year. In June and August more neutral storage lipids were synthesized, which hinted to a stress situation for the diatom mat (Guschina and Harwood 2006). The co-inertia analysis revealed that the observed metabolic change of the fate of carbon fixed by benthic diatoms in summer significantly correlated to low inorganic nutrient availability and high temperature and PAR. This is in line with the general idea that under unfavorable environmental conditions such as desiccation, nutrient deficiency, high light intensity, and/or high temperature, algae can alter their lipid biosynthetic pathways towards the formation and accumulation of neutral lipids, mainly in the form of triacylglycerides (TAGs) (Guschina and Harwood 2006; Fields et al. 2014; Levitan et al. 2015). Both temperature and PAR can fluctuate immensely at the sediment surface especially during the summer season (Serôdio and Catarino 1999). Produced TAGs do not perform a role as structural compound, but primarily serve as a storage form of carbon and energy (Hu et al. 2008). In addition, there is evidence suggesting that TAG synthesis plays a more active role in stress response of diatoms and may serve as an electron sink. Under stress conditions excess electrons that accumulated in the photosynthetic electron transport chain may induce excess of reactive oxygen species, which may in turn inhibit photosynthesis and cause damage to membrane lipids, protein and other macromolecules (Hu et al. 2008). To prevent this, diatoms form saturated FAs such as C18, which consumes approximately twice the NADPH derived from the electron transport chain that is required for the synthesis of a similar mass of CHO or protein (Hu et al. 2008). In addition, accumulation of lipids may be more advantageous during summer because lipids contain twice the energy stored per carbon atoms than that of CHOs and lipids save intracellular storage space due to their relative compactness (Rawat et al. 2013).

The observed RNA/DNA ratios were low in summer. This ratio has been taken as a proxy for metabolic activity and growth of microorganisms although this should be done with much caution (Blazewicz et al. 2013). With reservation, one could argue that this low RNA/DNA ratio hints to a lower growth rate in summer, which is indeed supported by the other results. It is unlikely that lower growth rates in summer are related to the exposure of high irradiance levels [possible in combination with high ultraviolet irradiance (Buma et al. 1996)], because Peletier et al. (1996) found that, in contrast to pelagic species, benthic diatoms are adapted to high irradiance levels and that their cell division rates are not influenced by it. However, the presumed environmental stress that the diatoms are exposed to (e.g., observed low inorganic nutrient concentrations) may have decreased the growth rate.

In addition to inorganic nitrogen, diatoms may use several sources of organic nutrients (Berman and Bronk 2003). For example, urea can be an important nitrogen source for microphytobenthos (Veuger and Middelburg 2007). Benthic fauna may exude urea that could serve as a source of nitrogen during summer when inorganic forms are unavailable (Therkildsen and Lomstein 1994). *C. volutator* and *P. ulvae* were present in high numbers in summer at the study site. If faunal excreted urea would indeed be an important nutrient in summer, it would explain the increase of PL1-SFA and PL1-MUFA at the expense of a lower synthesis of PL1-PUFA. The former are more saturated lipid-derived FAs and might play a role as part (or precursor) of urea transporters, also called 'lipid rafts' (Chen 2013). In addition, during summer the rate of arginine synthesis was higher. Arginine is an intermediate of the urea cycle (Armbrust et al. 2004) supporting the supposed importance of urea as a source of nitrogen for the diatoms (Allen et al. 2011; Prihoda et al. 2012). Hence, the lack of inorganic nitrogen and the possible switch to urea as well as the high temperature and PAR are main factors explaining the metabolic changes of the diatom mat during summer.

During high rates of carbon fixation (i.e., in February/April) a large part of the photo-assimilated carbon is excreted as EPS. Stal (2010) hypothesized that EPS are produced as the result of unbalanced growth (i.e., when fixed $CO_2$ is converted to intracellular storage CHO, but the capacity of storage is limited and the excess carbon fixation is exuded). Especially during the highly productive months of February and April, EPS production might function as outlet valve for excess energy. Subsequently, EPS production decreased during lower productive months in June, August, October and December, which confirms a close coupling between EPS production and photosynthesis and agrees with other reports (Pierre et al. 2014). A different function of excreted EPS between summer and other seasons could be hypothesized. The reason to exude carbon in February and April is presumably due to the above suggested nutrient diffusion limitation of the dense diatom mat and subsequent unbalanced growth. However, in summer the reason to exude carbon might be more related to motility as the diatom mat has to overcome the effects of bioturbation (e.g., sediment burial) and to avoid stressful conditions like high light levels in the very top of the sediment (Consalvey et al. 2004). EPS is an important factor in sediment stabilization (Stal 2010). Visual observations confirmed that cohesive sediment structures were obtained when a high percentage of the fixed carbon was excreted as EPS (i.e., in February, April, October, and December). In contrast, the sediment appeared less cohesive during summer. The high EPS loss that occurs within a day after the start of the experiment suggests that EPS was either consumed by bacteria (Goto et al. 2001), re-absorbed by the benthic diatoms (Miyatake et al. 2014), or washed away by tidal immersion (Hanlon et al. 2006). It should be noted

that different types of EPS are present in the sediment that are characterized by differences in recalcitrance to microbial degradation and potential to bind and stabilize sediment (de Brouwer and Stal 2001; Underwood and Paterson 2003). Acidic EPS (operational fraction extracted by EDTA) has a higher longevity and binds stronger to charged sediment particles and to itself. More neutral (containing a high proportion of glucose) EPS (operational fraction extracted by water) are more prone to microbial consumption. Whether that leads to the formation of the acidic fraction as suggested by Stal (2010) remains to be seen. In this research, EPS was treated as one single pool and functional roles of the different operational fractions were not considered.

The relative $^{13}C$ carbon pool proportioning of the diatom mat in October and December was similar as in February and April but the synthesis rate of all determined carbon pools was much lower in the former months. The high content of $\beta$-carotene and the increased light affinity coefficient ($\alpha$) suggested that the diatom mat was limited by light due to the shortening of the day lengths and the decreased irradiance at the end of the year. In addition, the low light angle of the sun would have reflected much of the light during these months of the year (Pinckney and Zingmark 1991). Together with chlorophyll the higher content of $\beta$-carotene extended the wavelength range of usable light for photosynthesis (Kuczynska et al. 2015). Chl *a* is the primary pigment for photosynthesis in diatoms, but the range of light absorption can be extended by inter alia $\beta$-carotene which increases the efficiency of photosynthesis by absorbing blue-green light and transferring this energy to chlorophyll (that absorbs mainly red-blue light) (Telfer 2002). In winter and especially in February, PUFA synthesis of the NL, PL1, and PL2 pools was important. We hypothesize that this served to maintain cell membrane fluidity and flexibility at lower temperatures (Jiang and Gao 2004; Sakthivel et al. 2011).

The diatom mat in this study was a compact and complex conglomerate up to 40 diatom taxa varying between seasons in species composition, size, motility, and productivity. Pigment signatures confirmed diatoms were the dominant microphytobenthic group of organisms. The visually observed variation in diatom density during the day and between months is probably due to daily migrations of the diatoms and biomass differences between months, respectively. It is known that the diatom community composition changes as a result of seasonal and multiannual variability in environmental conditions (Underwood and Barnett 2006). In this study, grazing could have been an important factor for the overall observed decrease of biomass in summer. Also seasonality in nutrient availability could have affected the composition of diatom assemblages as the growth rate of certain species are more affected by the available nitrogen source than others (Thornton et al. 2002; Litchman et al. 2009).

Although this study determined four major classes of organic compounds, there were still many compounds outside the analytical window, such as amino sugars, lectins, acidic CHOs, pigments, and quinones. In addition, incomplete recovery and analytical limitations of the determination of the major classes of biopolymers may have added to the unexplained part of the $^{13}C$ TOC labeling (Lee et al. 2004). The biochemical composition of the sediment organic matter suggested that major amounts of detritus were present in the sediment and that therefore only a fraction was derived from living organisms. However, by combining the latest compound specific stable isotope techniques with in situ labeling this study showed major seasonal changes in the biosynthesis of major classes of organic compounds and in this way contributed to the unraveling of the metabolic pathways of photosynthetic acquired carbon within a diatom mat and their metabolic responses to changing condition through the year.

## References

Admiraal, W., H. Peletier, and T. Brouwer. 1984. The seasonal succession patterns of diatom species on an intertidal mudflat: An experimental analysis. Oikos **42**: 30–40. doi:10.2307/3544606

Allen, A. E., and others. 2011. Evolution and metabolic significance of the urea cycle in photosynthetic diatoms. Nature **473**: 203–207. doi:10.1038/nature10074

Armbrust, E. V., and others. 2004. The genome of the diatom *Thalassiosira pseudonana*: Ecology, evolution, and metabolism. Science **306**: 79–86. doi:10.1126/science.1101156

Barnett, A., and others. 2015. Growth form defines physiological photoprotective capacity in intertidal benthic diatoms. ISME J. **9**: 32–45. doi:10.1038/ismej.2014.105

Bellinger, B. J., G. J. C. Underwood, S. E. Ziegler, and M. R. Gretz. 2009. Significance of diatom-derived polymers in carbon flow dynamics within estuarine biofilms determined through isotopic enrichment. Aquat. Microb. Ecol. **55**: 169–187. doi:10.3354/ame01287

Bender, S. J., M. S. Parker, and E. V. Armbrust. 2012. Coupled effects of light and nitrogen source on the urea cycle and nitrogen metabolism over a diel cycle in the marine diatom *Thalassiosira pseudonana*. Protist **163**: 232–251. doi:10.1016/j.protis.2011.07.008

Berman, T., and D. A. Bronk. 2003. Dissolved organic nitrogen: A dynamic participant in aquatic ecosystems. Aquat. Microb. Ecol. **31**: 279–305. doi:10.3354/ame031279

Blazewicz, S. J., R. L. Barnard, R. A. Daly, and M. K. Firestone. 2013. Evaluating rRNA as an indicator of microbial activity in environmental communities: Limitations and uses. ISME J. **7**: 2061–2068. doi:10.1038/ismej.2013.102

Boschker, H. T. S., J. F. C. de Brouwer, and T. E. Cappenberg. 1999. The contribution of macrophyte-derived organic matter to microbial biomass in salt-marsh sediments: Stable

carbon isotope analysis of microbial biomarkers. Limnol. Oceanogr. **44**: 309–319. doi:10.4319/lo.1999.44.2.0309

Boschker, H. T. S., T. C. W. Moerdijk-Poortvliet, P. van Breugel, M. Houtekamer, and J. J. Middelburg. 2008. A versatile method for stable carbon isotope analysis of carbohydrates by high-performance liquid chromatography/isotope ratio mass spectrometry. Rapid Commun. Mass Spectrom. **22**: 3902–3908. doi:10.1002/rcm.3804

Bouillon, S., and H. T. S. Boschker. 2006. Bacterial carbon sources in coastal sediments: A cross-system analysis based on stable isotope data of biomarkers. Biogeosciences **3**: 175–185. doi:10.5194/bg-3-175-2006

Brown, M., S. Jeffrey, J. Volkman, and G. Dunstan. 1997. Nutritional properties of microalgae for mariculture. Aquaculture **151**: 315–331. doi:10.1016/S0044-8486(96)01501-3

Buma, A. G. J., E. J. van Hannen, M. J. W. Veldhuis, and W. W. C. Gieskes. 1996. UV-B induces DNA damage and DNA synthesis delay in the marine diatom *Cyclotella* sp. Sci. Mar. **60**: 101–106.

Cahoon, L. B. 1999. The role of benthic microalgae in neritic ecosystems. Oceanogr. Mar. Biol. Ann. Rev. **37**: 47–86.

Chen, G. 2013. New advances in urea transporter UT-A1 membrane trafficking. Int. J. Mol. Sci. **14**: 10674–10682. doi:10.3390/ijms140510674

Chessel, D., A. Dufour, and J. Thioulouse. 2004. The ade4 package. I. One-table methods. R News **4**: 5–10.

Como, S., C. Lefrancois, E. Maggi, F. Antognarelli, and C. Dupuy. 2014. Behavioral responses of juvenile golden gray mullet *Liza aurata* to changes in coastal temperatures and consequences for benthic food resources. J. Sea Res. **92**: 66–73. doi:10.1016/j.seares.2013.10.004

Consalvey, M., D. M. Paterson, and G. J. C. Underwood. 2004. The ups and downs of life in a benthic biofilm: Migration of benthic diatoms. Diatom Res. **19**: 181–202. doi:10.1080/0269249X.2004.9705870

Cowie, G. L., and J. I. Hedges. 1984. Determination of neutral sugars in plankton, sediments, and wood by capillary gas-chromatography of equilibrated isomeric mixtures. Anal. Chem. **56**: 497–504. doi:10.1021/ac00267a046

de Brouwer, J. F. C., and L. J. Stal. 2001. Short-term dynamics in microphytobenthos distribution and associated extracellular carbohydrates in surface sediments of an intertidal mudflat. Mar. Ecol. Prog. Ser. **218**: 33–44. doi:10.3354/meps218033

de Jonge, V. N. 1980. Fluctuations in the organic carbon to Chl *a* ratios for estuarine benthic diatom populations. Mar. Ecol. Prog. Ser. **2**: 345–353. doi:10.3354/meps002345

Degré, D., and others. 2006. Comparative analysis of the food webs of two intertidal mudflats during two seasons using inverse modelling: Aiguillon Cove and Brouage Mudflat, France. Estuar. Coast. Shelf Sci. **69**: 107–124. doi:10.1016/j.ecss.2006.04.001

Dijkman, N. A., and J. C. Kromkamp. 2006. Phospholipid-derived fatty acids as chemotaxonomic markers for phytoplankton: Application for inferring phytoplankton composition. Mar. Ecol. Prog. Ser. **324**: 113–125. doi:10.3354/meps324113

Dolédec, S., and D. Chessel. 1994. Co-inertia analysis: An alternative method for studying species-environment relationships. Freshw. Biol. **31**: 277–294. doi:10.1111/j.1365-2427.1994.tb01741.x

Dray, S., D. Chessel, and J. Thioulouse. 2003. Co-inertia analysis and the linking of ecological data tables. Ecology **84**: 3078–3089. doi:10.1890/03-0178

Eilers, P. H. C., and J. C. H. Peeters. 1988. A model for the relationship between light intensity and the rate of photosynthesis in phytoplankton. Ecol. Model. **42**: 199–215. doi:10.1016/0304-3800(88)90057-9

Escoufier, Y. 1973. Le traitement des variables vectorielles. Biometrics **29**: 751–760. doi:10.2307/2529140

Evrard, V., P. L. M. Cook, B. Veuger, M. Huettel, and J. J. Middelburg. 2008. Tracing carbon and nitrogen incorporation and pathways in the microbial community of a photic subtidal sand. Aquat. Microb. Ecol. **53**: 257–269. doi:10.3354/ame01248

Fields, M. W., and others. 2014. Sources and resources: Importance of nutrients, resource allocation, and ecology in microalgal cultivation for lipid accumulation. Appl. Microbiol. Biotechnol. **98**: 4805–4816. doi:10.1007/s00253-014-5694-7

Goto, N., T. Kawamura, O. Mitamura, and H. Terai. 1999. Importance of extracellular organic carbon production in the total primary production by tidal-flat diatoms in comparison to phytoplankton. Mar. Ecol. Prog. Ser. **190**: 289–295. doi:10.3354/meps190289

Goto, N., O. Mitamura, and H. Terai. 2001. Biodegradation of photosynthetically produced extracellular organic carbon from intertidal benthic algae. J. Exp. Mar. Biol. Ecol. **257**: 73–86. doi:10.1016/S0022-0981(00)00329-4

Guschina, I. A., and J. L. Harwood. 2006. Lipids and lipid metabolism in eukaryotic algae. Prog. Lipid Res. **45**: 160–186. doi:10.1016/j.plipres.2006.01.001

Hanlon, A. R. M. and others. 2006. Dynamics of extracellular polymeric substance (EPS) production and loss in an estuarine, diatom-dominated, microalgal biofilm over a tidal emersion-immersion period. Limnol. Oceanogr. **51**: 79–93. doi:10.4319/lo.2006.51.1.0079

Heinzelmann, S. M., N. J. Bale, E. C. Hopmans, J. S. Sinninghe Damsté, S. Schouten, and M. T. J. van der Meer. 2014. Critical assessment of glyco-and phospholipid separation by using silica chromatography. Appl. Environ. Microb. **80**: 360–365. doi:10.1128/AEM.02817-13

Heo, M., and K. R. Gabriel. 1998. A permutation test of association between configurations by means of the RV coefficient. Commun. Stat. Simul. Comput. **27**: 843–856. doi:10.1080/03610919808813512

Herman, P. M. J., J. J. Middelburg, J. van de Koppel, and C. H. R. Heip. 1999. Ecology of estuarine macrobenthos. Adv. Ecol. Res. **29**: 195–240.

Herman, P. M. J., J. J. Middelburg, J. Widdows, C. H. Lucas, and C. H. R. Heip. 2000. Stable isotopes as trophic tracers: combining field sampling and manipulative labelling of food resources for macrobenthos. Mar. Ecol. Progr. Ser. **204**: 79–92. doi:10.3354/meps204079

Hillebrand, H., C. D. Dürselen, D. Kirschtel, U. Pollingher, and T. Zohary. 1999. Biovolume calculation for pelagic and benthic microalgae. J. Phycol. **35**: 403–424. doi:10.1046/j.1529-8817.1999.3520403.x

Hockin, N. L., T. Mock, F. Mulholland, S. Kopriva, and G. Malin. 2012. The response of diatom central carbon metabolism to nitrogen starvation is different from that of green algae and higher plants. Plant. Physiol. **158**: 299–312. doi:10.1104/pp.111.184333

Hu, Q., M. Sommerfeld, E. Jarvis, M. Ghirardi, M. Posewitz, M. Seibert, and A. Darzins. 2008. Microalgal triacylglycerols as feedstocks for biofuel production: Perspectives and advances. Plant J. **54**: 621–639. doi:10.1111/j.1365-313X.2008.03492.x

Jiang, H., and K. Gao. 2004. Effects of lowering temperature during culture on the production of polyunsaturated fatty acids in the marine diatom *Phaeodactylum tricornutum* (Bacillariophyceae). J. Phycol. **40**: 651–654. doi:10.1111/j.1529-8817.2004.03112.x

Jones, R. H., and K. J. Flynn. 2005. Nutritional status and diet composition affect the value of diatoms as copepod prey. Science **307**: 1457–1459. doi:10.1126/science. 1107767

Kromkamp, J. C., and R. M. Forster. 2003. The use of variable fluorescence measurements in aquatic ecosystems: Differences between multiple and single turnover measuring protocols and suggested terminology. Eur. J. Phycol. **38**: 103–112. doi:10.1080/0967026031000094094

Kroth, P. G., and others. 2008. A model for carbohydrate metabolism in the diatom *Phaeodactylum tricornutum* deduced from comparative whole genome analysis. PLoS One **3**: e1426. doi:10.1371/journal.pone.0001426

Kuczynska, P., M. Jemiola-Rzeminska, and K. Strzalka. 2015. Photosynthetic pigments in diatoms. Mar. Drugs **13**: 5847–5881. doi:10.3390/md13095847

Lee, C., S. Wakeham, and C. Arnosti. 2004. Particulate organic matter in the sea: The composition conundrum. AMBIO **33**: 565–575. doi:10.1639/0044-7447(2004)033[0565:POMITS]2.0.CO;2

Levitan, O., and others. 2015. Remodeling of intermediate metabolism in the diatom *Phaeodactylum tricornutum* under nitrogen stress. Proc. Natl. Acad. Sci. USA **112**: 412–417. doi:10.1073/pnas.1419818112

Litchman, E., C. Klausmeier, and K. Yoshiyama. 2009. Contrasting size evolution in marine and freshwater diatoms. Proc. Natl. Acad. Sci. USA **106**: 2665–2670. doi:10.1073/pnas.0810891106

MacIntyre, H. L., and J. J. Cullen. 1996. Primary production by suspended and benthic microalgae in a turbid estuary: Time-scales of variability in San Antonio Bay, Texas. Mar. Ecol. Progr. Ser. **145**: 245–268. doi:10.3354/meps145245

McCullagh, J. S. O., D. Juchelka, and R. E. M. Hedges. 2006. Analysis of amino acid $^{13}C$ abundance from human and faunal bone collagen using liquid chromatography/isotope ratio mass spectrometry. Rapid Commun. Mass Spectrom. **20**: 2761–2768. doi:10.1002/rcm.2651

Middelburg, J. J., C. Barranguet, H. T. S. Boschker, P. M. J. Herman, T. Moens, and C. H. R. Heip. 2000. The fate of intertidal microphytobenthos carbon: An in situ $^{13}C$-labeling study. Limnol. Oceanogr. **45**: 1224–1234. doi:10.4319/lo.2000.45.6.1224

Mitbavkar, S., and A. C. Anil. 2004. Vertical migratory rhythms of benthic diatoms in a tropical intertidal sand flat: Influence of irradiance and tides. Mar. Biol. **145**: 9–20. doi:10.1007/s00227-004-1300-3

Miyajima, T., Y. Yamada, Y. T. Hanba, K. Yoshii, T. Koitabashi, and E. Wada. 1995. Determining the stable isotope ratio of total dissolved inorganic carbon in lakewater by GC/C/IRMS. Limnol. Oceanogr. **40**: 994–1000. doi:10.4319/lo.1995.40.5.0994

Miyatake, T., T. C. W. Moerdijk-Poortvliet, L. J. Stal, and H. T. S. Boschker. 2014. Tracing carbon flow from microphytobenthos to major bacterial groups in an intertidal marine sediment by using an in situ $^{13}C$ pulse-chase method. Limnol. Oceanogr. **59**: 1275–1287. doi:10.4319/lo.2014.59.4.1275

Moerdijk-Poortvliet, T. C. W., L. J. Stal, and H. T. S. Boschker. 2014*a*. LC/IRMS analysis: A powerful technique to trace carbon flow in microphytobenthic communities in intertidal sediments. J. Sea Res. **92**: 19–25. doi:10.1016/j.seares.2013.10.002

Moerdijk-Poortvliet, T. C. W., J. Brasser, G. Ruiter, M. Houtekamer, H. Bolhuis, L. J. Stal, and H. T. S. Boschker. 2014*b*. A versatile method for simultaneous stable carbon isotope analysis of DNA and RNA nucleotides by liquid chromatography/isotope ratio mass spectrometry. Rapid Commun. Mass Spectrom. **28**: 1401–1411. doi:10.1002/rcm.6919

Oakes, J. M., B. D. Eyre, J. J. Middelburg, and H. T. S. Boschker. 2010. Composition, production, and loss of carbohydrates in subtropical shallow subtidal sandy sediments: Rapid processing and long-term retention revealed by $^{13}C$-labeling. Limnol. Oceanogr. **55**: 2126–2138. doi:10.4319/lo.2010.55.5.2126

Peletier, H., W. W. C. Gieskes, and A. G. J. Buma. 1996. Ultraviolet-B radiation resistance of benthic diatoms isolated from tidal flats in the Dutch Wadden Sea. Mar. Ecol. Progr. Ser. **135**: 163–168. doi:10.3354/meps135163

Pierre, G., J.-M. Zhao, F. Orvain, C. Dupuy, G. L. Klein, M. Graber, and T. Maugard. 2014. Seasonal dynamics of extracellular polymeric substances (EPS) in surface sediments of a diatom-dominated intertidal mudflat (Marennes–Oléron, France). J. Sea Res. **92**: 26–35. doi:10.1016/j.seares.2013.07.018

Pinckney, J., and R. G. Zingmark. 1991. Effects of tidal stage and sun angles on intertidal benthic microalgal productivity. Mar. Ecol. Progr. Ser. **76**: 81–89. doi:10.3354/meps076081

Pniewski, F., P. Biskup, I. Bubak, P. Richard, A. Latala, and G. Blanchard. 2015. Photo-regulation in microphytobenthos from intertidal mudflats and non-tidal coastal shallows. Estuar. Coast. Shelf Sci. **152**: 153–161. doi:10.1016/j.ecss.2014.11.022

Prihoda, J., A. Tanaka, W. B. M. de Paula, J. F. Allen, L. Tirichine, and C. Bowler. 2012. Chloroplast-mitochondria cross-talk in diatoms. J. Exp. Bot. **63**: 1543–1557. doi:10.1093/jxb/err441

R Development Core Team. 2015. R: A language and environment for statistical computing. R Foundation for Statistical Computing, Vienna, Austria.

Rawat, I., R. Ranjith Kumar, T. Mutanda, and F. Bux. 2013. Biodiesel from microalgae: A critical evaluation from laboratory to large scale production. Appl. Energy **103**: 444–467. doi:10.1016/j.apenergy.2012.10.004

Sabbe, K., A. Witkowski, and W. Vyverman. 1995. Taxonomy, morphology and ecology of *Biremis lucens* comb. nov.(Bacillariophyta): A brackish-marine, benthic diatom species comprising different morphological types. Bot. Mar. **38**: 379–392. doi:10.1515/botm.1995.38.1-6.379

Sakthivel, R., S. Elumalai, and M. M. Arif. 2011. Microalgae lipid research, past, present: A critical review for biodiesel production, in the future. J. Exp. Sci. **2**: 29–49.

Serôdio, J., and F. Catarino. 1999. Fortnightly light and temperature variability in estuarine intertidal sediments and implications for microphytobenthos primary productivity. Aquat. Ecol. **33**: 235–241.

Serôdio, J., S. Vieira, S. Cruz, and F. Barroso. 2005. Short-term variability in the photosynthetic activity of microphytobenthos as detected by measuring rapid light curves using variable fluorescence. Mar. Biol. **146**: 903–914. doi:10.1007/s00227-004-1504-6

Smith, D. J., and G. J. C. Underwood. 2000. The production of extracellular carbohydrates by estuarine benthic diatoms: The effects of growth phase and light and dark treatment. J. Phycol. **36**: 321–333. doi:10.1046/j.1529-8817.2000.99148.x

Stal, L. J. 2010. Microphytobenthos as a biogeomorphological force in intertidal sediment stabilization. Ecol. Eng. **36**: 236–245. doi:10.1016/j.ecoleng.2008.12.032

Stewart, P. S. 2003. Diffusion in biofilms. J. Bacteriol. **185**: 1485–1491. doi:10.1128/JB.185.5.1485-1491.2003

Taylor, J. D., B. A. McKew, A. Kuhl, T. J. McGenity, and G. J. C. Underwood. 2013. Microphytobenthic extracellular polymeric substances (EPS) in intertidal sediments fuel both generalist and specialist EPS-degrading bacteria. Limnol. Oceanogr. **58**: 1463–1480. doi:10.4319/lo.2013.58.4.1463

Telfer, A. 2002. What is *β*–carotene doing in the photosystem II reaction centre? Phil. Trans. R. Soc. Lond. B. **357**: 1431–1440. doi:10.1098/rstb.2002.1139

Therkildsen, M. S., and B. A. Lomstein. 1994. Seasonal variation in sediment urea turn-over in a shallow estuary. Mar. Ecol. Progr. Ser. **109**: 77–82. doi:10.3354/meps109077

Thornton, D. C. O., L. F. Dong, G. J. C. Underwood, and D. B. Nedwell. 2002. Factors affecting microphytobenthic biomass, species composition and production in the Colne Estuary (UK). Aquat. Microb. Ecol. **27**: 285–300. doi:10.3354/ame027285

Underwood, G. J. C., and J. Kromkamp. 1999. Primary production by phytoplankton and microphytobenthos in estuaries. Adv. Ecol. Res. **29**: 93–153.

Underwood, G. J. C., and D. M. Paterson. 2003. The importance of extracellular carbohydrate production by marine epipelic diatoms. Adv. Bot. Res. **40**: 183–240. doi:10.1016/S0065-2296(05)40005-1

Underwood, G. J. C., R. G. Perkins, M. C. Consalvey, A. R. M. Hanlon, K. Oxborough, N. R. Baker, and D. M. Paterson. 2005. Patterns in microphytobenthic primary productivity: Species-specific variation in migratory rhythms and photosynthetic efficiency in mixed-species biofilms. Limnol. Oceanogr. **50**: 755–767. doi:10.4319/lo.2005.50.3.0755

Underwood, G. J. C., and M. Barnett. 2006. What determines species composition in microphytobenthic biofilms? p. 123–140. *In* J.C. Kromkamp, J.F.C. de Brouwer, G.F. Blanchard, R.M. Forster, and V. Créach [eds.], Functioning of microphytobenthos in estuaries. Royal Netherlands Academy of Arts and Sciences.

van Oevelen, D., K. Soetaert, J. J. Middelburg, P. M. J. Herman, L. Moodley, I. Hamels, T. Moens, and C. H. R. Heip. 2006. Carbon flows through a benthic food web: Integrating biomass, isotope and tracer data. J. Mar. Res. **64**: 453–482. doi:10.1357/002224006778189581

Veuger, B., J. J. Middelburg, H. T. S. Boschker, and M. Houtekamer. 2005. Analysis of $^{15}N$ incorporation into D-alanine: A new method for tracing nitrogen uptake by bacteria. Limnol. Oceanogr.: Methods **3**: 230–240.

Veuger, B., and J. J. Middelburg. 2007. Incorporation of nitrogen from amino acids and urea by benthic microbes: Role of bacteria versus algae and coupled incorporation of carbon. Aquat. Microb. Ecol. **48**: 35–46. doi:10.3354/ame048035

## Acknowledgments

We thank Erwin Moerdijk, Wanda Moerdijk, Jelle Moerdijk, Jurian Brasser and Gerjan de Ruiter for assisting in the field sample collection and processing of samples in the laboratory.

## Conflict of Interest

None declared.

*Submitted 10 January 2017*
*Revised 22 May 2017*
*Accepted 10 July 2017*

*Associate editor: Josette Garnier*